Int. J. Electrochem. Sci., 3 **(2008)** 489-508

International Journal of ELECTROCHEMICAL SCIENCE
www.electrochemsci.org

Passivation and Cl^- Induced Depassivation of Cu-Ag Alloys in Borate Buffer Solutions

Omar A. Hazzazi[1,], Ayman M. Zaky[2] , Mohammed A. Amin[3] and Sayed S. Abd El Rehim[3]*

[1] Chemistry Department, Faculty of Applied Science, Umm Al-Qura University, Makkah, Saudi Arabia.
[2] Chemistry Department, Faculty of Science, South Valley University, Qena 83523, Egypt.
[3] Chemistry Department, Faculty of Science, Ain Shams University, Abbasia, Cairo, Egypt.
[*]E-mail: hazazi@hotmail.com

Received: 15 December 2007 / *Accepted:* 7 February 2008 / *Online published:* 20 February 2008

The electrochemical behaviour of two Cu-Ag alloys, namely (20wt%Cu + 80wt%Ag) and (80wt%Cu + 20wt%Ag) alloys, was studied in 0.15 M borax and 0.15 M boric acid buffer solution, pH =8.45, by means of cyclic voltammetry, potentiodynamic anodic polarization and current/ time transients techniques. SEM and XRD microanalysis were used to examine the changes caused by the electrochemical perturbations. The anodic portion of the voltammogram was characterized by the existence of two potential regions I and II. In the first potential region copper dissolves preferentially and exhibits three anodic peaks A_1, A_2 and A_3. The anodic peak A_1 was related to the formation of Cu_2O, while the anodic peaks A_2 and A_3 are related to the oxidation of Cu and Cu_2O to CuO and $Cu(OH)_2$, respectively. The preferential dissolution of copper was enhanced and the simultaneous dissolution of silver was retarded on increasing the silver content in the alloy. The potential region II was characterized by the appearance of four anodic peaks A_5, A_6, A_7 and A_8 related to the formation of mono-layer, and multi-layers of Ag_2O, AgO and Ag_2O_3, respectively. The cathodic portion of the voltammogram was characterized by the appearance of six cathodic peaks C_1, C_2, C_3, C_4, C_5 and C_6 prior to hydrogen evolution reaction. The addition of small amount of Cl^- ion resulted in the appearance of two anodic peaks $A^{/}$ and $A^{//}$ due to the formation of $CuCl_2.H_2O$ and AgCl on the electrode surface, respectively. SEM examinations, in presence of Cl^- ions, confirmed the existence of pits on the alloy surface. Potentiostatic current/time transients showed that the formation of Cu_2O, CuO and $Cu(OH)_2$ involves a nucleation and growth mechanism under diffusion control. Potentiostatic measurements also showed that the overall anodic processes can be described by three stages. The first stage corresponds to the nucleation and growth of a passive oxide layer. The second and the third stages involve pit nucleation and growth, respectively. Nucleation of pit takes place after an incubation time (t_i). The rate of pit nucleation, defined as (t_i^{-1}), increases with increase in Cl^- concentration and applied step anodic potential ($E_{s,a}$).

Keywords: Cu-Ag alloys, borate buffer, chloride ion, pitting corrosion, cyclic voltammetry, current-time transients, SEM and XRD

1. INTRODUCTION

Coatings containing Cu-Ag alloys are highly used in low power circuits used in electronics due to their higher electrical and thermal conductivity compared to those of pure copper or pure silver [1]. Alloying with copper conserves silver and reduces costs [1]. There have been a few studies reported on the dissolution behaviour of metals from copper-silver alloys. The dissolution of silver, copper and silver-copper alloys was studied in acid and cyanide solutions using oxygen or ferric ion as an oxidant [2], in sulphuric acid [3] or in aerated ammoniacal solution [4, 5]. The electrochemical behaviour of Cu-Ag system was studied using different electrochemical techniques such as cyclic voltammetry, potentiodynamic anodic polarization and current time transients in Na_2CO_3 [6], in Na_2CO_3 containing Cl^- ion [7], in NaOH [8] and in NaOH containing sulphide ions [9]. The electrochemical behaviour of these alloys depends on their composition, as well as the composition of the electrolytic solution. In solutions free from additives, galvanic coupling played an important role in enhancing the dissolution of the less noble component, copper, and retarded the more noble component, silver. The addition of chloride or sulphide ions to the electrolytic solution had pronounced effect on altering the electrochemical behaviour of this system. Some authors have investigated the influence of borate anion on the metal dissolution and passivation processes and considered this anion to be a corrosion inhibitor, mainly for iron and steel, and have explained its performance as a pH controller buffer [10-17].

Only a few authors have considered the borate anion as an adsorption inhibitor [11-14, 18]. From this view point and depending on the buffering effect of borate solution and on the ability of boric acid to block the active center on the electrode surface a study of such a system on borate buffer solution with or without chloride ions was arisen to inspect the corrosion of these alloys. Scanning electron microscope was used to monitor pitting corrosion due to the addition of chloride ions. X-ray diffraction analysis was used to determine the composition of the corrosion products on the electrode surface.

2. EXPERIMENTAL

The working electrodes employed in the present work consisted of pure Cu and Ag (supplied by Merck 99.99%), and two Cu-Ag alloys, one containing 20 % by weight Ag (alloy I) and the other containing 80 % by weight Ag (alloy II). The two alloys were prepared by fusion of pure Cu and Ag constituents in a graphite crucible as recommended. The constitution of the two alloys was maintained using X-ray fluorescence analysis. All the working electrodes used were rods of an exposed area of 0.5 cm^2 embedded in Teflon so that only the cross-sectional area was in contact with the solution. Prior to each experiment, the surface pretreatment of the working electrode was performed by mechanical polishing (using a polishing machine model POLIMENT I, BUEHLER POLISHER) of the electrode surface with successive grades of emery papers down to 1200 grit up to a mirror finish. The electrode was then, rinsed with acetone, distilled water, and finally dipped in the electrolytic cell.

A potential of -1600 mV in relation to a saturated calomel electrode (SCE) was applied for 10 min in the same working solution for reduction of air-formed films. A conventional electrochemical cell of 200 ml capacity was used in the present work. It contained three separate compartments of

which two were used for fitting the working and the counter electrodes. The third compartment was used for fitting the reference electrode, which was a saturated calomel electrode (SCE). The counter electrode was a graphite rod of large surface area (10 cm^2). The solutions used were prepared from AnalaR grade chemicals and used without further purification. All experiments were performed using freshly prepared solutions and freshly polished electrodes.

Table 1 - Composition of the materials used

No.	***Electrode***	Composition wt%	
		Copper	Silver
1	Alloy I	20.0	80.0
2	Alloy II	80.0	20.0

The electrochemical experiments were conducted using an EG&G Galvanostat/Potentiostat Model 273A connected to a PII PC computer that used M352 SoftCorr II program. The potentiodynamic current/potential curves were recorded by changing the electrode potential, including compensation for the ohmic drop potential of the solution, automatically from the starting potential up to 1400 mV (SCE) with the required scanning rate. Cyclic voltammetry measurements were carried out by sweeping linearly the potential from the starting potential into the positive direction at a given scan rate till a required potential value and then reversed with the same scan rate till the starting potential to form one complete cycle.

The potentiostatic current/time transient measurements were carried out after a two step procedure, namely: the working electrode was first held at the starting potential for 10 min to attain a reproducible electroreduced electrode surface. Then the electrode was suddenly polarized in the positive direction to a step anodic potential, $E_{s,a}$, at which the current transient was recorded.

Surface morphology of the alloy I polarized to more noble potentials was obtained using scanning electron microscopy (SEM), model XL-200 Philips operated at 20 keV. The composition of the corrosion products formed during anodic polarization over the electrode surface was examined by means of X-ray diffraction analysis using Philips P. W. Model 1730 diffractometer adopted at 40 kV and 25 mA with Cu-k_α radiation and a Ni filter.

3. RESULTS AND DISCUSSIONS

3.1. Cyclic voltammetry of pure Cu, Ag and the two Cu-Ag alloys in borate buffer solutions

Figure 1, curve 2 represents a typical cyclic voltammogram recorded for the copper electrode in 0.15 M borax and 0.15 M boric acid buffer solution (pH 8.45) at a scan rate of 50 mV s^{-1} and at 25^0 C. Three anodic, namely A_1, A_2 and A_3, and two cathodic, namely C_1 and C_2, peaks were obtained [19].

According to Pourbaix [20], the following oxidation equilibria are possible for copper/ aqueous solution system:

$$2Cu + H_2O = Cu_2O + 2H^+ + 2e^- \qquad E = -269 \text{ mV} \qquad (1)$$
$$Cu + H_2O = CuO + 2H^+ + 2e^- \qquad E = -170 \text{ mV} \qquad (2)$$
$$Cu + 2H_2O = Cu(OH)_2 + 2H^+ + 2e^- \qquad E = -131 \text{ mV} \qquad (3)$$
$$Cu_2O + H_2O = 2CuO + 2H^+ + 2e^- \qquad E = -71 \text{ mV} \qquad (4)$$
$$Cu_2O + 3H_2O = 2Cu(OH)_2 + 2H^+ + 2e^- \qquad E = 7 \text{ mV} \qquad (5)$$

Accordingly, the anodic current peak A_1 was attributed to the electroformation of a Cu_2O layer, Equation 1, whereas the anodic peaks A_2 and A_3 are ascribed to the formation of a complex hydrous CuO film, Equations 2-5, resulting in a duplex structure of a passive film [21-36]. Such a structure represented by an outer $CuO/Cu(OH)_2$ layer overlaying a barrier Cu_2O. The reverse scan shows two cathodic current peaks C_2 and C_1 which are related to the reduction of CuO and $Cu(OH)_2$ to Cu_2O and Cu_2O to Cu, respectively.

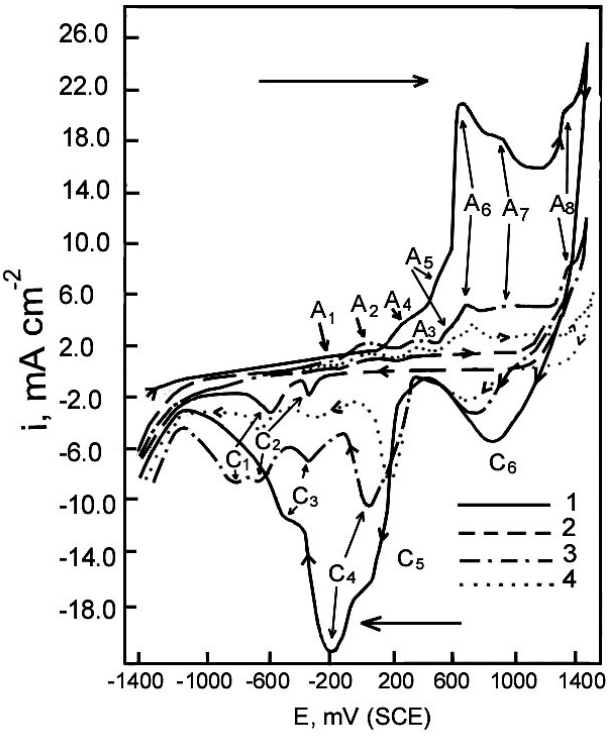

Figure 1. Cyclic voltammograms recorded for (1) silver; (2) copper; (3) alloy I; and (4) alloy II in 0.15 M borax and 0.15 M boric acid buffer solution (pH 8.45), at a scan rate of 50 mV s^1 andat 25 ^oC.

Figure 1, curve 1 shows a typical cyclic voltammogram recorded for an Ag electrode in 0.15 M borax and 0.15 M boric acid buffer solution at 25 ^oC at a scan rate of 50 mV s^{-1}. The anodic portion of the voltammogram was characterized by the existence of two potential regions, namely the active and the passive regions. The active region consists of five anodic peaks A_4, A_5, A_6, A_7 and A_8. The first anodic peak A_4 can be assigned to the anodic oxidation of Ag to $[Ag(OH)_2]^-$ soluble compound by adsorption

of OH^- and desorption of the products [37-39]:

$$Ag + 2OH^- = [Ag(OH)_2]^- + e^- \qquad \text{peak } A_4 \qquad (6)$$

When the concentration of this complex exceeds the solubility product of Ag_2O, precipitation of a monolayer of this oxide occurs on the electrode surface. The second peak (A_5) located at about 420 mV was related to the direct formation of Ag_2O monolayer on Ag surface.

$$2Ag + 2OH^- = Ag_2O + H_2O + 2e^- \qquad \text{peak } A_5 \qquad (7)$$

The anodic peak A_6 could be attributed to the formation of Ag_2O multilayers via nucleation and growth mechanisms [340-42]. The anodic peak A_7 is related to the oxidation of Ag_2O to AgO according to the following reaction [37, 43, 44]:

$$Ag_2O + 2OH^- = 2AgO + H_2O + 2e^- \qquad \text{peak } A_7 \qquad (8)$$

The anodic peak A_8 located prior to oxygen evolution reaction may be ascribed to the oxidation of AgO to higher oxidation state of silver, Ag_2O_3 [40, 45-48]:

$$2AgO + 2OH^- = Ag_2O_3 + H_2O + 2e^- \qquad \text{peak } A_8 \qquad (9)$$

The reverse scan of potential exhibited four cathodic current peaks C_3, C_4, C_5 and C_6 prior to hydrogen evolution reaction. The cathodic peak C_6 was related to the reduction of Ag_2O_3 to AgO. Also, the cathodic peak C_5 is due to the reduction of AgO to Ag_2O. The cathodic peaks C_4 and C_3 are related to the reduction of Ag_2O and AgO to Ag, respectively.

Curves 3 and 4, Fig. 1, represent cyclic voltammograms recorded for alloys I and II in 0.15 M borax and 0.15 M boric acid buffer solution at 25 ^oC at a scan rate of 50 mV s^{-1}, respectively. Inspection of these two cyclic voltammograms revealed that on positive going scan, the anodic portion of the voltammograms exhibited two potential regions; I and II. Within the potential range of region I, copper dissolves preferentially from the alloy resulting in the appearance of three anodic current peaks A_1, A_2 and A_3. It has been shown that these anodic peaks are related to the oxidation of Cu in the alloy to Cu_2O (peak A_1; Equation 10), CuO and/or $Cu(OH)_2$ (peak A_2; Equations 11 and 12) and Cu_2O to CuO and/or $Cu(OH)_2$ (peak A_3; Equations 4 and 5), respectively [21-36] via the following reactions:

$$Cu_x\text{-}Ag_y + H_2O = Cu_{x-2}\text{-}Ag_y + Cu_2O + 2H^+ + 2e^- \qquad \text{peak } A_1 \qquad (10)$$
$$Cu_{x-2}\text{-}Ag_y + H_2O = Cu_{x-3}\text{-}Ag_y + CuO + 2H^+ + 2e^- \qquad \text{peak } A_2 \qquad (11)$$
$$Cu_{x-3}\text{-}Ag_y + 2H_2O = Cu_{x-4}\text{-}Ag_y + Cu(OH)_2 + 2H^+ + 2e^- \qquad \text{peak } A_2 \qquad (12)$$

The current densities of the anodic peaks A_1, A_2 and A_3, namely j_{pA1}, j_{pA2} and j_{pA3}, were increased and their corresponding peak potentials, namely E_{pA1}, E_{pA2} and E_{pA3}, were shifted towards more negative (active) values with increasing silver content in the alloy. These results indicate that the dissolution of copper from the alloy is enhanced. This behaviour could be ascribed to the galvanic coupling effect [2-4]. The potential range of region II was characterized by the appearance of four anodic peaks A_5, A_6,

A_7 and A_8. The anodic peaks A_5 and A_6 were shown to be related to the formation of mono and multilayers of Ag_2O (Equation 13), respectively [40-42].

$$Cu_{x-4}\text{-}Ag_y + 2OH^- = Ag_2O + Cu_{x-4}\text{-}Ag_{y-2} + H_2O + 2e^- \qquad \text{peak } A_5 \qquad (13)$$

The anodic peak A_7 could be ascribed to the formation of AgO (Equation 8) [37, 43, 44]. The anodic peak A_8 could be related to the oxidation of AgO to higher oxidation state of silver, Ag_2O_3 (Equation 9) [40, 35-48]. Within the potential range of region II, increasing Cu content in the alloy drifts the potential of the anodic peaks towards more positive (noble) values. This may be due to the galvanic coupling effect of copper and silver in the alloys [2-3]. X-ray diffraction analysis, Fig. 2, of the alloy I surface anodically polarized to 1400 mV showed the existence of Ag_2O_3 with preferred orientation (111, 420), CuO with preferred orientation (220, -202) and $Cu(OH)_2$ with preferred orientation (002, 150). The reverse scan was characterized by the appearance of six cathodic peaks C_1, C_2, C_3, C_4, C_5 and C_6 prior to hydrogen evolution reaction.

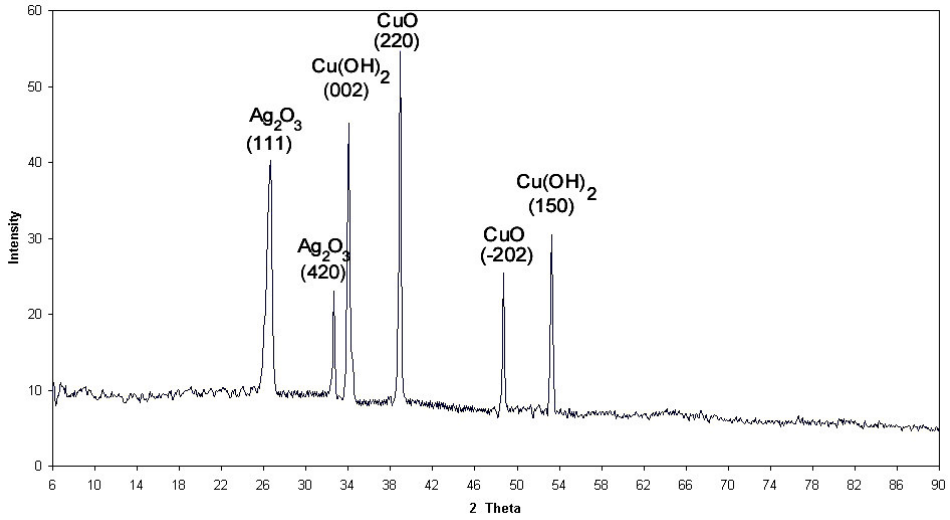

Figure 2. X-ray diffraction pattern recorded for alloy I surface after anodic polarization up to 1400 mV in 0.15 M borax and 0.15 M boric acid buffer solution (pH 8.45) at 25 ^oC.

3.2. Effect of potential reversing limit ($E_{s,a}$)

The effect of potential reversing limit, $E_{s,a}$, was used to distinguish the correlation between the anodic and cathodic peaks and is maintained by switching the anodic potential at different potential values. The voltammograms in Fig. 3 were obtained for alloy I in 0.15 M borax and 0.15 M boric acid buffer solution (pH 8.45) at a scan rate of 50 mV s^{-1} and at 25 ^oC.

It follows from the data of Fig. 3 that, reversal of the anodic potential limit, namely $E_{s,a}$, at a potential value beyond that of the anodic peak A_1 resulted in the appearance of one cathodic peak C_1. This results demonstrates that the cathodic peak C_1 is in conjugation with the anodic peak A_1 and is related to the reduction of Cu_2O layer to Cu. Switching $E_{s,a}$ at a potential value more positive than either that of the anodic peak A_2 or A_3 resulted in the appearance of two cathodic peaks C_1 and C_2. The

cathodic peak C_2 is therefore in conjugation with the anodic peaks A_2 and A_3 and is related to the reduction of both of CuO and $Cu(OH)_2$ to Cu_2O. When $E_{s,a}$ was reversed at a potential value positive to that of the anodic peaks A_4 or A_5, three cathodic peaks C_1, C_2 and C_3 appeared. The cathodic peak C_3 could be connected to the reduction of $[Ag(OH)_2]^-$ and/or Ag_2O to Ag. A new cathodic peak C_5 appeared when the anodic potential limit was reversed at a potential value positive to that of the anodic peak A_7 and is related to the reduction of AgO to Ag_2O. The cathodic peak C_6 appeared only when the anodic potential limit was reversed at potential values positive to that of the anodic peak A_8, and hence they are in conjugation. The cathodic peak C_6 may be related to the reduction of higher oxidation state Ag_2O_3 to AgO.

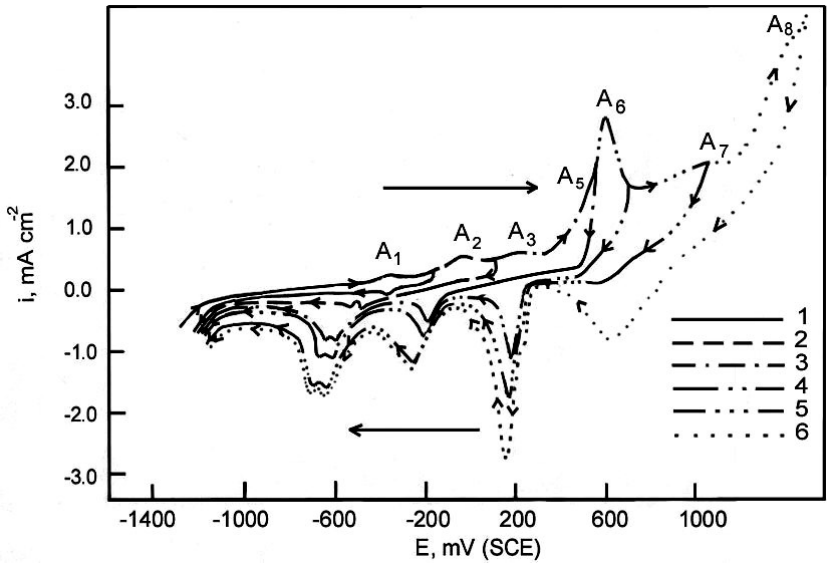

Figure 3. Typical first cyclic voltammetric scan for alloy I in 0.15 M borax and 0.15 M boric acid buffer solution (pH 8.45) at 25 ^oC and at a scan rate of 50 mV s^{-1}, starting from E_c = -1600 mV and being reversed at various step anodic potentials: $E_{s,a}$: (1) -200 mV; (2) 100 mV; (3) 550 mV; (4) 700 mV; (5) 1050 mV; (5) 1400 mV.

3.3. Effect of potential scan rate

The effect of potential scan rate on the cyclic voltammograms recorded for the two alloys was studied in 0.15 M borax and 0.15 M boric acid buffer solution (pH 8.45) at 25 ^oC. Figure 4 represents the voltammogram obtained for alloy I, as an example, under the effect of various scan rates. Similar results were obtained for alloy II (data not shown here). Inspection of Fig. 4 reveals that on increasing scan rate, the peak current density of all the anodic and cathodic peaks were increased. In addition, the anodic peak potentials were shifted to more positive (noble) direction while those of the cathodic peaks were shifted to less negative (noble) values. Figures 5 and 6 represent the linear dependence of the peak current density of the anodic peaks on the square root of the scan rate, $\nu^{1/2}$, for the two alloys, respectively.

Straight lines passing through the origin are obtained for the anodic peaks A_1 and A_2, meaning that processes associated with these two anodic peaks are under diffusion control. However, straight lines, with an intercept, are obtained for the anodic peaks, A_5, A_6, A_7 and A_8 which points to some

kinetic control contribution (mixed-control process). For a diffusion control processes, the linear dependence of the peak current density on the root of scan rate is given by Delahy [49] following Equation 14:

$$i_p = a \,.\, b.\, z^{1/2} \,.\, c.\, D^{1/2} \,.\, \nu^{1/2} \qquad (14)$$

where *a* and *b* are constants, *D* is the diffusion coefficient of the diffusing species and *z* is the number of the exchanged electrons.

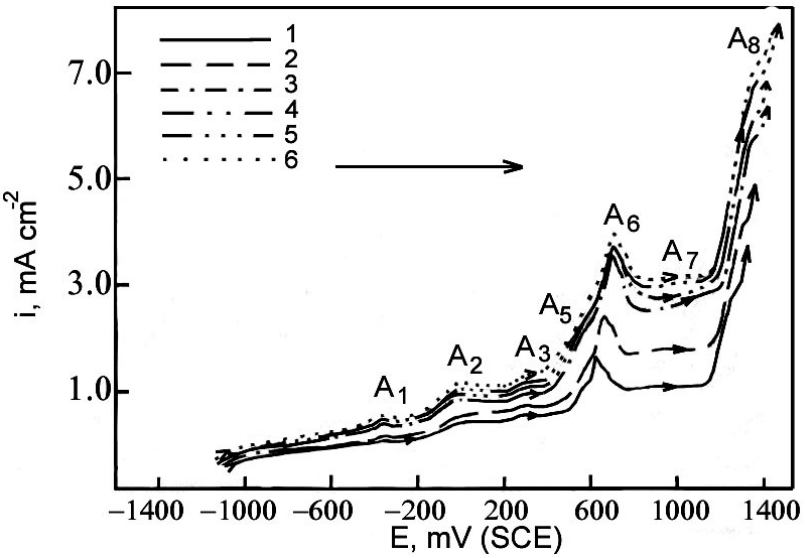

Figure 4. Typical first cyclic voltammetric scan for alloy I in 0.15 M borax and 0.15 M boric acid buffer solution (pH 8.45) at 25 ^{o}C and different scan rates: (1) 10 mV s^{-1}; (2) 25 mV s^{-1}; (3) 50 mV s^{-1}; (4) 75 mV s^{-1}; (5) 100 mV s^{-1}; (6) 125 mV s^{-1}.

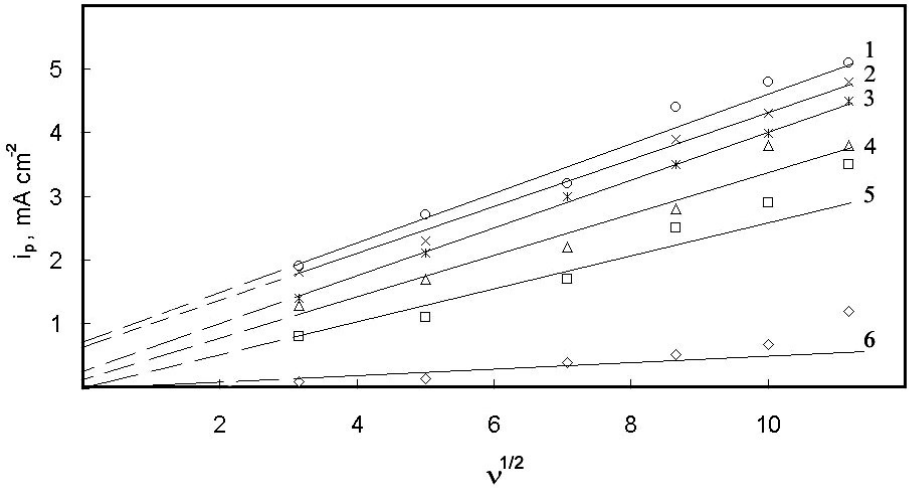

Figure 5. Dependence of the peak current density i_p on the square root of the potential scan rate for alloy I in 0.15 M borax and 0.15 M boric acid buffer solution (pH 8.45) at 25 ^{o}C: (1) peak A_8; (2) peak A_6; (3) peak A_7; (4) peak A_5; (5) peak A_2; (6) peak A_1.

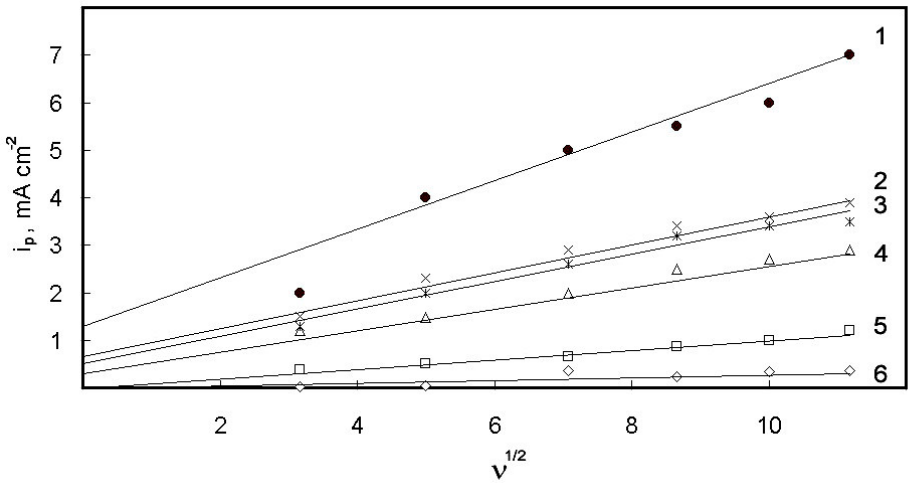

Figure 6. Dependence of the peak current density i_p on the square root of the potential scan rate for alloy II in 0.15 M borax and 0.15 M boric acid buffer solution (pH 8.45) at 25 ^oC: (1) peak A_8; (2) peak A_6; (3) peak A_7; (4) peak A_5; (5) peak A_2; (6) peak A_1.

3.4. Effect of Cl$^-$ ion addition

The influence of addition of increasing concentrations of NaCl (0.01 – 0.15 M) on the voltammograms of alloy I in 0.15 M borax and 0.15 M boric acid buffer solution (pH 8.45) at 25 ^oC was represented by curves (2-8) in Fig. 7.

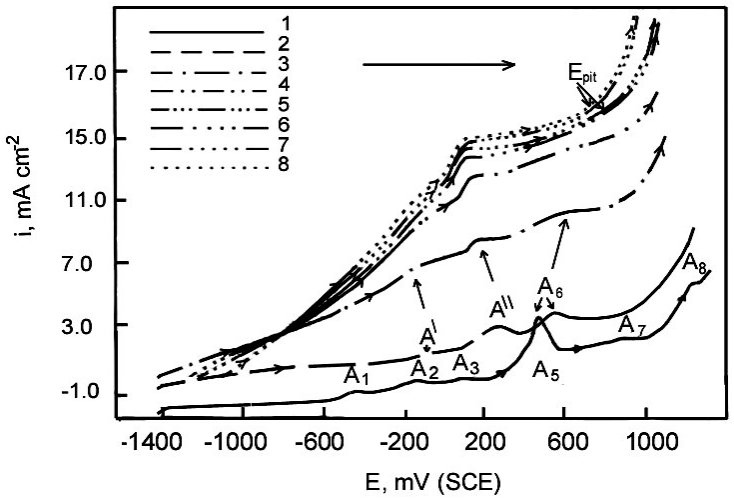

Figure 7. Typical first cyclic voltammetric scan recorded for alloy I in 0.15 M borax and 0.15 M boric acid buffer solution (pH 8.45) containing various concentrations of NaCl at 25 ^oC and at a scan rate of 50 mV s^{-1}: (1) blank; (2) 0.01 M; (3) 0.02 M; (4) 0.03 M; (5) 0.05 M; (6) 0.07 M; (7) 0.13 M; (8) 0.15 M.

The initial observation that is associated with the addition of increasing concentrations of Cl^- ions in the solution was shifting the zero current potential (E_{corr}) to more negative values. It is obvious that, upon the addition of increasing concentrations of Cl^- ions, all the anodic peaks A_1-A_8 were completely

disappeared, and new two anodic peaks $A^{/}$ and $A^{//}$ are observed. This behaviour may be related to the decrease in the dissolution of the alloy constituents in the vicinity of these anodic peaks, which could be ascribed to the competitive adsorbability [50-53] between Cl^- ions (essential for passivity breakdown and alloy dissolution) and OH^- ions (essential for passive layer formation) on the alloy surface. This competition reduced the concentration of OH^- ion at the metal surface with increasing Cl^- ion concentration, and this will, undoubtedly, favour passivity breakdown and retard passive layer formation. The heights of the anodic peak $A^{/}$ and $A^{//}$ were increased and their peak potentials were shifted towards more negative values with further increase in the Cl^- ion concentration. It seems that Cl^- ion is likely to become adsorbed on the metal surface forming a potentially active dissolution site and the subsequent anodic dissolution process through the anodic peaks $A^{/}$ and $A^{//}$ involves the formation of $CuCl_2$ and AgCl via Equations 15 and 16 [54, 55]:

$$Cu + 2Cl^- + 2H_2O \rightarrow CuCl_2.H_2O + 2e^- \qquad \text{peak } A^{/} \qquad (15)$$

$$Cu_x\text{-}Ag_y + Cl^- \rightarrow Cu_x\text{-}Ag_{y-1} + AgCl + e^- \qquad \text{peak } A^{//} \qquad (16)$$

When the concentration of Cl^- ion in solution reaches 0.05 M, the anodic current density beyond the anodic peak $A^{//}$ started to increase rapidly to a very high value, indicating passivity breakdown and initiation of pitting attack. The potential corresponding to the rapid increase in current is known as the pitting potential, E_{pit}. This potential was shifted towards more negative (active) values as the concentration of Cl^- ion in the solution was increased. Figure 8 shows the linear dependence of the pitting potential, E_{pit}, of alloy I on logarithm of the concentration of NaCl [log (C_{NaCl} / M)] in the solution according to the Equation:

$$E_{pit} = a - b \log C_{NaCl} \qquad (17)$$

Where a and b are constants.

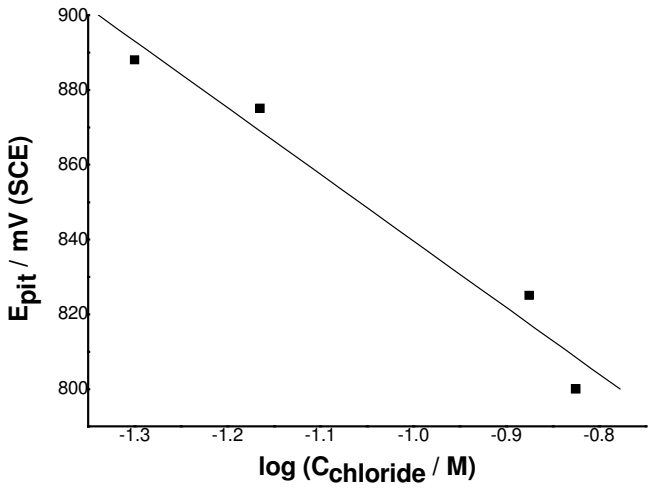

Figure 8. Linear dependence of the pitting potential (E_{pit}) on log (C_{NaCl} / M) for the alloy I in 0.15 M borax and 0.15 M boric acid buffer solution (pH 8.45) containing various concentrations of NaCl at 25 ^oC.

This relation is analogous to the phenomena that are commonly recognized in the studies of pitting corrosion on some metals and alloys the presence of some aggressive anions [56, 57]. The SEM image presented in Fig. 9 confirmed the existence of some pits on alloy I surface after anodic polarization from –1600 mV to 1170 mV in 0.15 M borax and 0.15 M boric acid buffer solution (pH 8.45) containing 0.05 M Cl^- ion.

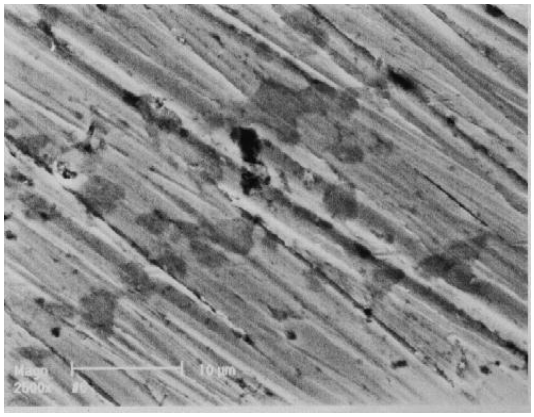

Figure 9. SEM micrograph (2500X) for alloy I surface after anodic polarization from –1600 mV to 1170 mV in in 0.15 M borax and 0.15 M boric acid buffer solution (pH 8.45) containing various concentrations of NaCl at 25 ^oC.

3.5. Current/ time (j/t) transient measurements

3.5.1. j/t measurements in absence of Cl^- ion

In order to get more information about the electrochemical behaviour of Cu-Ag system in 0.15 M borax and 0.15 M boric acid buffer solution (pH 8.45), potentiostatic current/time transients measurements were conducted for alloy I at different step anodic potentials, $E_{s,a}$. Figure 10 shows the current transients recorded for alloy I at 25 ^oC. Similar results were obtained for alloy II (data not shown here).

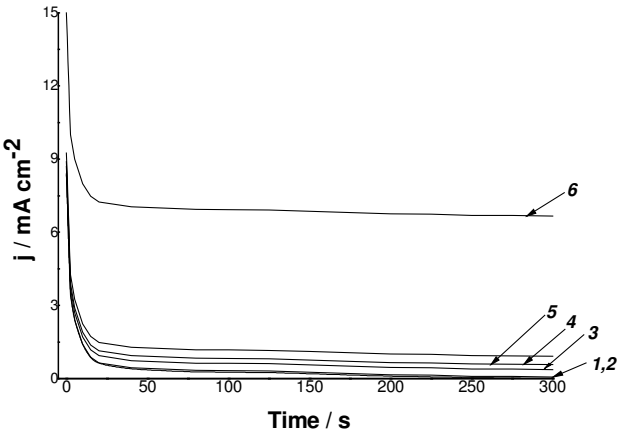

Figure 10. Current/time (j/t) transients recorded for alloy I in 0.15 M borax and 0.15 M boric acid buffer solution (pH 8.45) at 25 ^oC and at different step anodic potentials ($E_{s,a}$):(1) -350 mV; (2) 0.0 mV; (3) 300 mV; (4) 700 mV; (5) 1150 mV; (6) 1350 mV.

It is obvious that the instantaneous current transient densities decrease monotonically with time until reaches a steady state value. The values of the instantaneous and steady state current increase as $E_{s,a}$ is made more positive, indicating an increase in the thickness of the anodically formed layers. Plotting the current i vs. $t^{-1/2}$ for the continuously decreasing parts of the current transients (Fig. 11) gives straight lines with different slopes and features, depending on the values of $E_{s,a}$.

When $E_{s,a}$ is located within the potential range of peak A_1, a straight line passing through the origin is obtained (curve 6). For $E_{s,a} = E_{peak}$ of A_2 or A_3, the obtained plots (curves 4 and 5, respectively) consists of two straight portions. The data are consistent with the formation of two anodic layers {Cu_2O and (CuO - $Cu(OH)_2$)}with two different potential ranges. This result confirms results obtained from section 3.3 that processes associated with these anodic peaks are under diffusion control. On the other hand, If $E_{s,a}$ locates within the potential range of peak A_6, the plot consists of four portions with the first having an intercept (i.e., not passing through the origin), indicating a mixed-controlled process. This portion is related o the formation of Ag_2O mulilayers. The other three portions are consistent with the formation of three layers, namely Cu_2O, CuO/ $Cu(OH)_2$ and a monolayer of Ag_2O. Increasing $E_{s,a}$ above the potential range of peak A_7 gives plots consisting of five portions indicating the formation of five layers with five different potential ranges with the first one not passing through the origin. These findings indicate the occurrence of a mixed-controlled process. This portion is in consistent with the formation of AgO. The other four portions are related to the formation of layers of Cu_2O, CuO, a monolayer of Ag_2O and mulilayers of Ag_2O, respectively. When $E_{s,a}$ is in the potential region of the anodic peak A_8, the plot consists of six portions indicating the formation of six different anodic layers with the first portion not passing through the origin and was related to the formation of Ag_2O_3. These results suggest that the formation of Cu_2O, CuO and $Cu(OH)_2$ involve nucleation and growth mechanisms under mixed-control.

3.5.2. j/t measurements in presence of Cl^- ion

The objective of this section is to throw more light on the role of aggressive Cl^- ions in the kinetics of passivity breakdown and initiation of pitting attack of the two alloys in borate buffer solutions. For this purpose, j/t measurements were made at constant $E_{s,a}$ under different experimental conditions. The effect of $E_{s,a}$ (in the range between 0 and 1400 mV) on the current vs. time transients of the two alloys in 0.15 M borax and 0.15 M boric acid buffer (blank) solution (pH =8.45) containing 0.05 M NaCl were studied. Figure 12 collects results obtained for alloy I; similar results were obtained for alloy II. The results showed that in the absence of halide ions (curve 1), the transient current decreases rapidly at first and then tends to attain a steady state value. The decrease in the currents are related to, as discussed in details in the previous section, nucleation and growth of the passive films on the anode surface. These data indicate that in blank solution, the two alloys can be polarized anodically without showing any evidence of pitting corrosion. However, in the presence of Cl^- ions (curves 2-9), the current/time curves depend on the value of $E_{s,a}$. For $E_{s,a} < E_{pit}$ (curves 2-4), the current density decreases to a steady state value, indicating that for these step anodic potentials, the Cl^- ions are not sufficient to breakdown the passive layer. In this case, if the contribution of the double layer charging

process is neglected, the overall transient current density (j) can be related to two main processes, namely the passive layer growth (j_{gr}) and the alloy electrodissolution through the passive layer (j_{dis}):

$$j = j_{gr} + j_{dis} \quad (18)$$

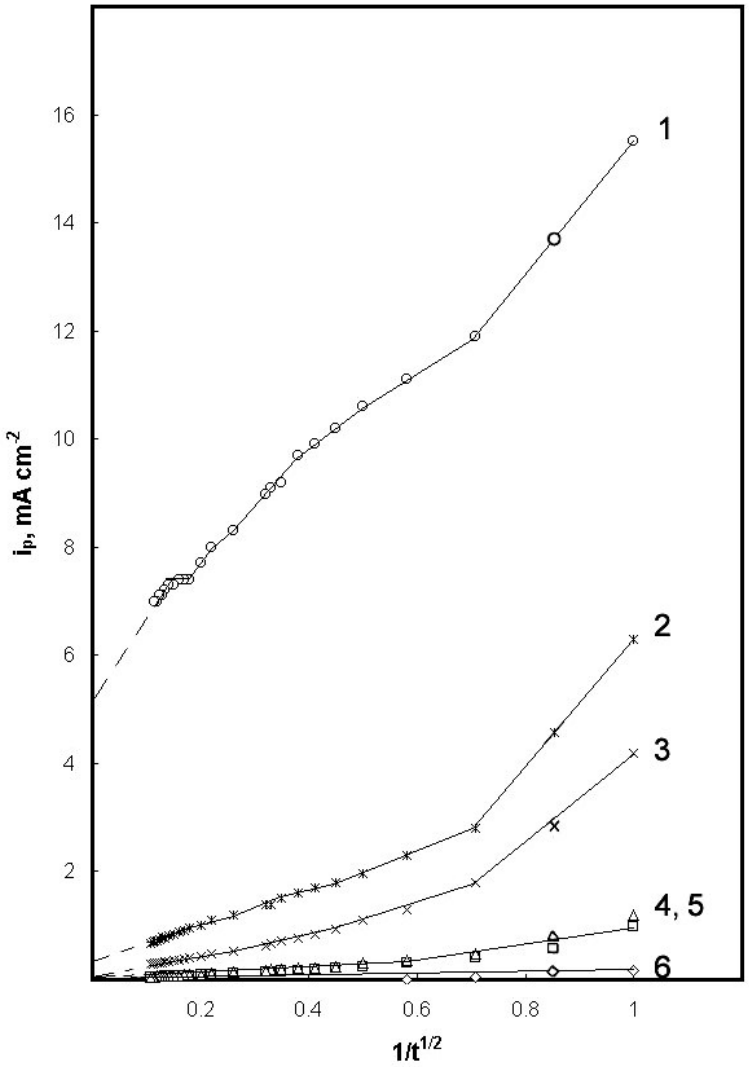

Figure 11. Dependence of the current density on $t^{-1/2}$ for descending portions of the current transients for alloy I in 0.15 M borax and 0.15 M boric acid buffer solution (pH 8.45) at 25 ^{o}C and at different step anodic potentials ($E_{s,a}$): (1) -350 mV; (2) 0.0 mV; (3) 300 mV; (4) 700 mV; (5) 1150 mV; (6) 1350 mV.

The growth of the passive layer, as previously mentioned, can be assigned to the formation of a passive layer (solid phase) on the electrode surface. The electrodissolution of the anode through the passive layer can be explained in terms of cation diffusion from the metal/film interface to the film/solution interface. These two processes can proceed independently on the entire electrode surface.

It seems that the rate of these two processes are nearly the same at the steady state current so as to keep the thickness of the passive film nearly constant.

On the other hand, For $E_{s,a} > E_{pit}$ (curves 5-9) the transient current density initially decreases to a minimum value at a certain incubation time, t_i, and then increases. The general trend of an increasing current suggests that pit growth is the dominant process and a number of well-developed pits could be observed following this active period (as seen in SEM images). The incubation time is caused by the time required for local removal of the passive film via the sequence of Cl^- adsorption, penetration and formation of a readily soluble complexes. Later, pit growth, and consequently the sudden rise in the transient current density is observed. In this case, the overall transient current density is given by three contributions:

$$j = j_{gr} + j_{dis} + j_{pit} \qquad (19)$$

j_{pit} is related to the pit growth current density. Further experiments were performed to clarify the influence of Cl^- ions concentration on the current transients of the two alloys at $E_{s,a}$ = 1200 mV (1200 mV > E_{pit} for each sample). Some results are given in Fig. 13.

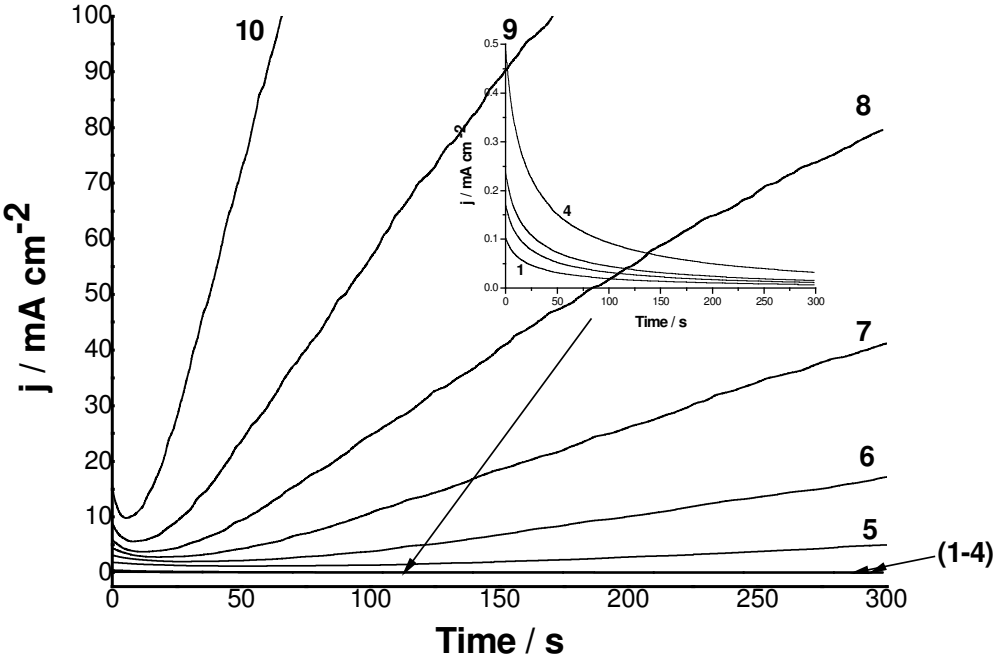

Figure 12. Effect of step anodic potential, $E_{s,a}$, on the current/time (j/t) transients recorded for alloy I in 0.15 M borax and 0.15 M boric acid buffer solution (pH 8.45) containing 0.05 M NaCl at 25 ^oC. (1) $E_{s,a}$ = 0.0 mV; (2) $E_{s,a}$ = 200 mV; (3) $E_{s,a}$ = 400 mV; (4) $E_{s,a}$ = 600 mV; (5) $E_{s,a}$ = 800 mV; (6) $E_{s,a}$ = 1000 mV; (7) $E_{s,a}$ = 1100 mV; (8) $E_{s,a}$ = 1200 mV; (9) $E_{s,a}$ = 1300 mV; (10) $E_{s,a}$ = 1400 mV.

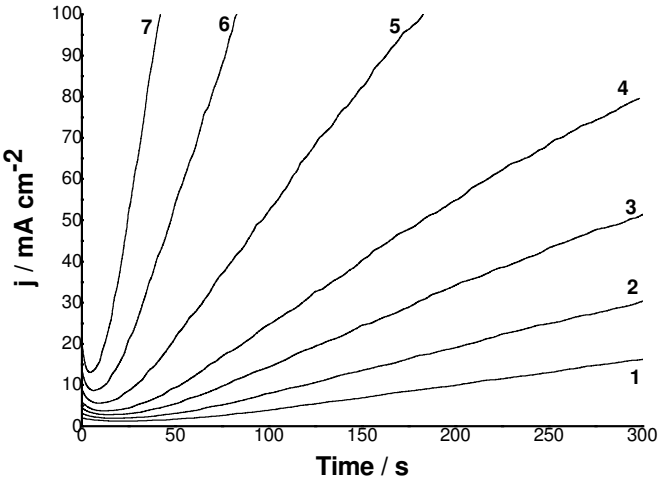

Figure 13. The influence of Cl^- ion concentration on the current/time (j/t) transients recorded for alloy I in 0.15 M borax and 0.15 M boric acid buffer solution (pH 8.45) containing at $E_{s,a}$ = 1200 mV and at 25 ^oC: (1) 0.01 M; (2) 0.02 M; (3) 0.03 M; (4) 0.05 M; (5) 0.07 M; (6) 0.13 M; (7) 0.15 M.

It follows from the data of Fig. 13 that the pit growth current density (j_{pit}) increases and the incubation time (t_i) becomes shorter, and therefore the rate of pitting attach enhances, with an increase in Cl^- ion concentration. It is found that the pit growth current density j_{pit} (the rising part of the transient) follows a current relationship with a square root of time, $t^{1/2}$, (Figs. 14 and 15 are representative examples).

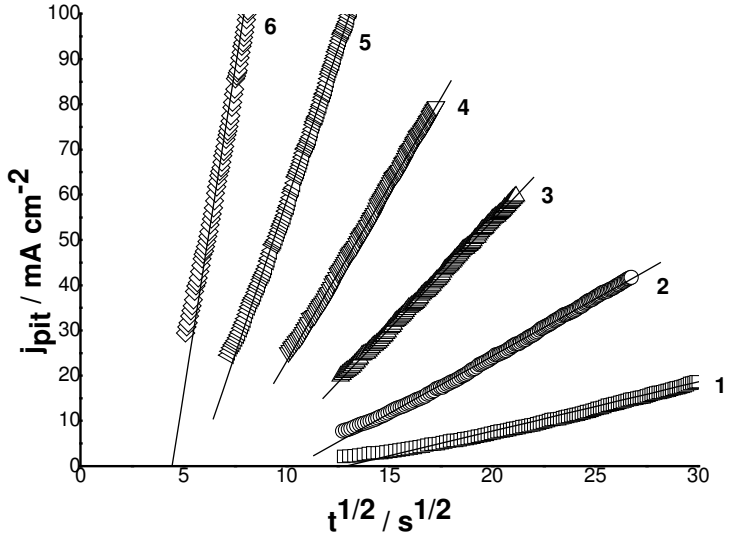

Figure 14. Dependence of pit growth current density (j_{pit}) on square root of time ($t^{1/2}$) recorded for alloy I in 0.15 M borax and 0.15 M boric acid buffer solution (pH 8.45) containing 0.05 M NaCl at 25 ^oC and at various step anodic potentials ($E_{s,a}$). (1) $E_{s,a}$ = 800 mV; (2) $E_{s,a}$ = 1000 mV; (3) $E_{s,a}$ = 1100 mV; (4) $E_{s,a}$ = 1200 mV; (5) $E_{s,a}$ = 1300 mV; (6) $E_{s,a}$ = 1400 mV.

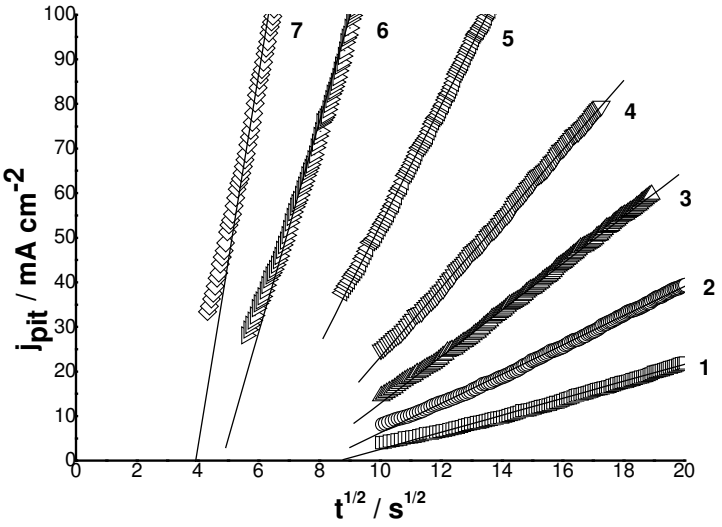

Figure 15. Dependence of pit growth current density (j_{pit}) on square root of time ($t^{1/2}$) recorded for alloy I in 0.15 M borax and 0.15 M boric acid buffer solution (pH 8.45) containing various concentrations of Cl^- ions at $E_{s,a}$ = 1200 mV and at 25 ^oC. (1)0.01 M; (2) 0.02 M; (3) 0.03 M; (4) 0.05 M; (5) 0.07 M; (6) 0.13 M; (7) 0.15 M.

The linear relationship suggests that the pit growth is an instantaneous three dimensional growth under diffusion control [58]. These results agree well with Hills model [59] which can be ascribed by the Equation:

$$j_{pit} = A\, t^{1/2} \qquad (20)$$

where $A = 2^{3/2}\, z\, F\, \pi\, N_o\, D^{3/2}\, C^{3/2}\, M^{1/2}\, \rho^{1/2}$, where N_o is the number of the sites available for pitting corrosion, D, C, M, and ρ are the diffusion coefficient, the concentration, the molecular weight, and the density of the dissolved materials and the other terms have their usual meaning. Regarding to the data of Figs. 14 and 15, it can be an interception on the axis at zero j_{pit} confirming that an incubation time is necessary before pit growth occurs. It is obvious that the incubation time t_i decreases (and hence the rate of pit growth, defined as t_i^{-1}, increases) with increasing $E_{s,a}$ and concentration of Cl^- ions. These observations can be confirmed by plotting t_i^{-1} for the two alloys vs. $E_{s,a}$ and concentration of Cl^- ions, as shown in Figs. 16 and 17, respectively. Figure 16 denotes that the rate of pit nucleation enhances with increasing $E_{s,a}$. These results agree well with the observations of Nisancioglu and Holtan [60]. The dependence of the rate of pit nucleation on $E_{s,a}$ suggests that there is a distribution of nucleation sites of different energies which nucleate at distinct potential [61]. In other words, the more positive is the applied potential, the more will be the active sites available for pit nucleation. Moreover, an increase in $E_{s,a}$ may increase the electric field across the passive film and therefore enhances the adsorption of the aggressive Cl^- ions on the passive electrode surface.

Complete inspection of Figs. 16 and 17 revealed that the rate of pit nucleation and growth under identical conditions decreases with increasing Cu content in the alloy. These results confirm those obtained from polarization measurements that alloy II (with the highest Cu content) showed the highest pitting corrosion resistance. Figure 17 infers that for each sample, the rate of pit nucleation increases with increasing the concentration of aggressive Cl^- ions.

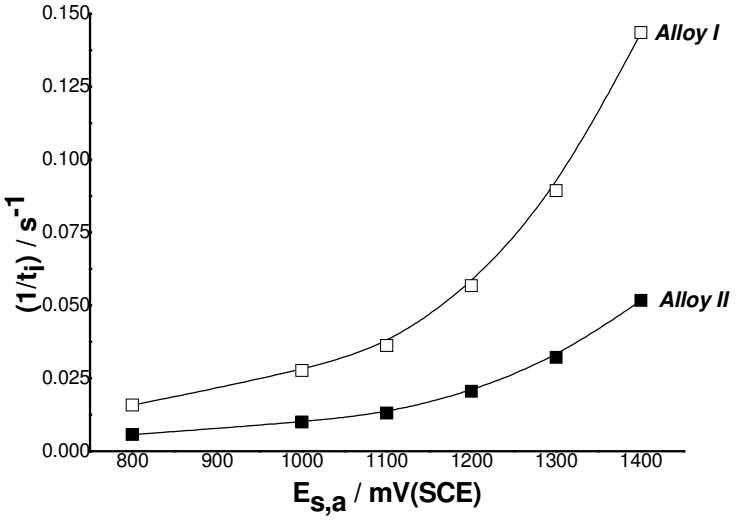

Figure 16. Relationship between the rate of pit growth ($1/t_i$) and step anodic potentials ($E_{s,a}$) recorded for the two alloys in 0.15 M borax and 0.15 M boric acid buffer solution (pH 8.45)containing 0.05 M NaCl at 25 ^oC.

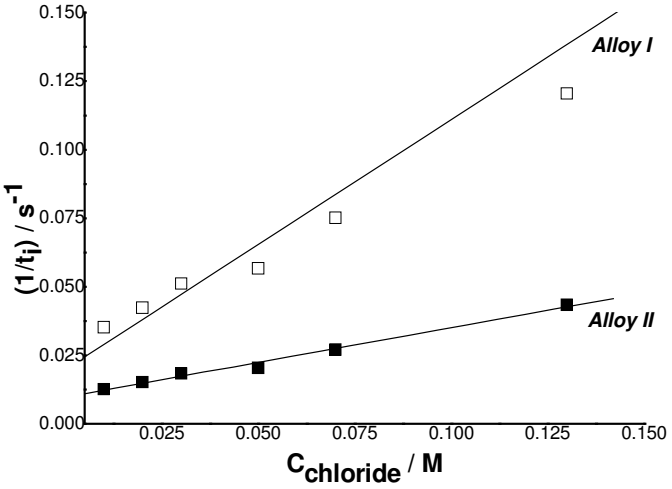

Figure 17. Relationship between the rate of pit growth ($1/t_i$) and Cl^- ion concentration ($C_{perchlorate}$) recorded for the two alloys in 0.15 M borax and 0.15 M boric acid buffer solution (pH 8.45) containing various concentrations of Cl^- ions at $E_{s,a}$ = 1200 mV and at 25 ^oC.

4. CONCLUSIONS

1. The electrochemical behaviour of Cu-Ag alloys in slightly alkaline borate solutions investigated depends on the anion present in solution. . In the presence of only borate, eight anodic peaks (A_1 - A_8), and six cathodic peaks (C_1-C_6) are observed. These anodic peaks in the medium containing only borate may be related to film formation reactions.
2. Current-time transients showed that the formation of Cu_2O, CuO and $Cu(OH)_2$ involve nucleation and growth mechanisms under diffusion control the formation of mono-layer and multi-layers of Ag_2O, AgO and Ag_2O_3 involves some kinetic control instead of pure diffusion control
3. X-ray diffraction analysis showed the existence of Ag_2O_3 with preferred orientation (111, 420), CuO with preferred orientation (220, -202) and $Cu(OH)_2$ with preferred orientation (002, 150) on the alloy I surface anodically polarized to 1400 mV.
4. Addition of chloride ion to borate solution resulted in a competitive adsorbability between Cl^- and OH^- ions at the alloy surface and changes the voltammetric profile. Two new anodic peaks $A^{/}$ and $A^{//}$ are observed and are related on the formation of $CuCl_2.H_2O$ and AgCl on the electrode surface respectively.
5. When chloride ion concentration reaches 0.05 M pitting attack started. Increasing he chloride ion concentration enhanced the pitting attack.
6. SEM micrograph obtained for alloy I surface in the vicinity of pitting potentials showed that the electrode surface suffered from pitting attack.

References

1. R. Lein, G. Bär, *Elektrie*, 33, No. 10 (1979) 511.
2. Y. U. Chai , E. C. Lee and K. N. Han, *Metallurgical transactions* B, 22B (1991) 755.
3. L. L. Tokar, T. A. Tarisyna, Y. S. Sorikov, M. S. Igumnov, S. A. Erofeev and C. D. Men'shikov, *Zhurnal Prikladnoi Khimii*, 63 (1990) 2638.
4. Y. Charles and K. N. Han, *Mineral Metall. Processing*, (1994) 12.
5. Y. Charles and K. N. Han, *J. Electrochem. Soc*., 142 (1995) 1819.
6. A. M. Zaky, *British Corros*. J. 36 (2001) 59.
7. A. M. Zaky, *Electrochimica Acta*, 51 (2006) 2057.
8. F. H. Assaf, A. M. Zaky and S. S. Abd El Rehim, 2002, *Appl. surf. Sci*. 187, no. 1-2, (2002) 18.
9. A. M. Zaky, S. S.Abd El Rehim and B. M. Mohamed*, Int. J. Electrochem. Sci*., 1 (2006) 17.
10. R.C. Bhardwaj, A.Gonzلlez-Martin and J.O'M. Bockris, *J. Electrochem. Soc*. 138 (1991) 1901.
11. J.A. Bardwell, B.J. MacDougall, *J. Electrochem. Soc*. 135(1988) 2157.
12. B. MacDougall, J.A. Bardwell, *J. Electrochem. Soc*. 135(1988) 2437.
13. T. Hurlen, S. Gunvaldsen, F. Blaker, *Electrochim. Acta* 29(1984) 1163.
14. M. Fischer, W. Gruner, G. Reinhardt, *Corros. Sci*. 15(1975) 275.
15. K. Ogura, *J. Electroanal. Chem*. 79(1977) 149.
16. R. Goetz, D.F. Mitchell, B. MacDougall, M.J. Graham, *J. Electrochem. Soc*. 134(1987) 535.
17. E.M.A. Martini, S.T. Amaral, I.L. Muller, *J. Braz. Chem. Soc*. 1995, 6, 77.
18. Emilse M.A. Martini, and Iduvirges L. Mullerb *J. Braz. Chem. Soc*., 10 (6) (1999)505
19. R. Babić, M. Metikoš-Huković and A. Jukić, *J. Elecrochem. Soc*., 148 (2001) B147.

20. M. Pourbaix, Atlas of Elecrochemical Equilibria in aqueous Solutions, Pregamon Press, New York (1966).
21. M. Yamashita, K. Omura and D. Hirayama, *Surf. Sci*., 96 (1980) 443.
22. M. J. Gennero de Chialvo, J. O. Zerbio, S. L. Marchiano and A. J. Arvia, *J. Appl. Electrochem*., 16 (1986) 517.
23. J. G. Becerra, R. C. Salvarezza and A. J. Arvia, *Electrochim. Acta,* 33 (1988) 613.
24. H. D. Strehblow and B. Titze, *Electrochim, Acta*, 25 (1980) 839.
25. M. M. Lohrengel, J. W. Schultze, H. D. Speckmann and H. H. Strehblow, *Electrochim. Acta* 32 (1987) 733.
26. M. Seo, X. C. Jiang and N. Sato, *Werks. Korros*., 39 (1988) 583.
27. Y. Feng, K. S. Siow, W. K. Teo, K. L. Tan and A. K. Hseih, *Corrosion*, 53 (1997) 389.
28. L. M. Abrantes, L. M. Castillo, C. Norman and L. M. Peter, *J. Electroanal. Chem*., 163 (1984) 209.
29. H. Y. H. Chan, C. G. Takoudis and M. J. Weaver, *J. Phys. Chem*. B, 103 (1999) 357.
30. S. Mayer and R. Muller, *J. Elecrtochem. Soc*., 139 (1992) 8426.
31. W. Kautek, M. Geus, M. Sahre, P. Zhao and Mirwald, *Surf. Interface Anal*., 255 (1997) 488.
32. L. D. Burke, M. J. G. Ahern and T. G. Ryan, *J. Elecrtochem. Soc*., 137 (1990) 533.
33. R. Babic, M. Metikos-Hukovic and M. Loncar, *Electrtochim. Aca*, 44 (1999) 2413.
34. R. Babic and M. Metikos-Hukovic, *Tin Solid Films*, 359 (2000) 88.
35. M. Metikos-Hukovic, K. Furic, R. Babic and A. Marinovic, *Surf. Interface Anal*., 27 (1999) 1016.
36. B. V. Tilak, R. S. Perkins, H. A. Kozlowska and B. E. Conway, *Electrochim. Acta* 17 (1972) 1447.
37. J. Ambrose, R. G. Barradas, *Electrochim. Acta*, 19 (1974) 781.
38. R. S. Perkins, B. V. Tilak, B. E. Conway and H. A. Kozlowska, *Electrochim. Acta*, 17 (1972) 1471.
39. A. M. Zaky, F. H. Assaf, S. S. Abd El Rehim and B. M. Mohamed, *Appl. Surf. Sci*., 221 (2004) 349.
40. R. F. Amlie, H. N. Honer and P. ?Ruetschi, *J. Electrochem. Soc*., 112 (1965) 1073.
41. G. T. Burstein, R. C. Newman, *Electrochim. Acta*, 25 (1980) 1009.
42. R. H. Muller, C. G. Smith, *Surf. Sci*. 96 (1980) 375.
43. T. P. Hoar, C. K. Dyer, *Electrochim. Acta*, 17 (1972) 1563.
44. P. Sonchart, *Electrochim. Acta* 13 (1988) 1789.
45. T. G. Clarke, N. A. Hampson, J. B. Lee, J. R. Morley and B. Scanlon, *Can. J. Chem*., 46 (1968) 3437.
46. B. Miller, *J. Electrochem. Soc.*, 117 (1970) 491.
47. N. A. Hampson, K. I. Mc Donald J. B. Lee*, J. Electroanal. Chem*. 45 (1973) 149.
48. D. W. Shoesmith, T. E. Rummery, D. Owen and W. Lee, *J. Electrochem. Soc.,* 123 (1976) 790.
49. P. Delahay "New instrumental methods in electrochemistry" , New york, NY, Wiley, 124; 1954.
50. H. Bohni and H. H. Uhlig, J. Electrochem. Soc. 116 (1969) 906.
51. R. P. Frankenthal and J. Kruger, "Passivity of Metals", The Electrochemical Society Inc., Princeton, New Jersey (1978).
52. K. E. Heusler, "Encyclopedia of Electrochemistry of The Elements", Vol. IX-A Marcel Dekker, New York (1982) 229-381.
53. W. J. Lorenz and K. E. Heusler, "Corrosion Mechanism" (edited by F. MANSFELD), Marcel Dekker, New York (1987) 1.
54. D. R. Lide and H. P. R. Frederikse, " Handbook of Chemistry and Physics", 75th edition, Chemical / Rubber Publishing Co. (CRC), USA (1994).
55. A. Nishikata, M. Iagaki, T. Tsuru, S. Haruyama and E. Fujii, *Corrosion Engineering* 39 (1990) 25.
56. S. S. Abd El Rehim, E. E. Fouad, S. M. Abd El Wahaab and H. H. Hassan*, J. Electroanal. Chem*. 401 (1996) 113.
57. S. A. M. Refaey and S. S. Abd El Reheim, *Electrochim. Acta* 42 (1996) 667.
58. S.S. Abdel Rehim, H.H. Hassan, M.A. Ibrahim, M.A. Amin, *Monatsh. Chem*. 130 (10) (1999) 1207.

59. G.J. Hills, D.J. Schiffin, J. Thompson, *Electrochim. Acta* 22 (1974) 448.
60. K. Nisancioglu, H. Holtan, *Corros. Sci*. 18 (1978) 835.
61. M. Metikos-Hukovic, *J. Appl. Electrochem*. 22 (1992) 448.